Atomic and electronic structure of the $SrNbO_3/SrNbO_{3.4}$ interface

Chunlin Chen,[1] Shuhui Lv,[1,2,a)] Zhongchang Wang,[1,b)] Kazuto Akagi,[1] Frank Lichtenberg,[3] Yuichi Ikuhara,[1,4,5,c)] and Johannes Georg Bednorz[6]
[1]*Advanced Institute for Materials Research, Tohoku University, 2-1-1 Katahira, Aoba-ku, Sendai 980-8577, Japan*
[2]*School of Materials Science and Engineering, Changchun University of Science and Technology, Changchun 130022, China*
[3]*Department of Materials, ETH Zürich, Zürich CH-8093, Switzerland*
[4]*Institute of Engineering Innovation, The University of Tokyo, 2-11-16 Yayoi, Bunkyo-ku, Tokyo 113-8656, Japan*
[5]*Nanostrctures Research Laboratory, Japan Fine Ceramic Center, Atsuta Ku, Nagoya, Aichi 4568587, Japan*
[6]*IBM Research Division, Zürich Research Laboratory, Rüschlikon CH-8803, Switzerland*

(Received 5 September 2014; accepted 16 November 2014; published online 1 December 2014)

We have determined the atomic-scale structure of the $SrNbO_3/SrNbO_{3.4}$ interface and related it to the electronic structure. Experimentally, transmission electron microscopy observations reveal that $SrNbO_3$ and $SrNbO_{3.4}$ show orientation relationships $[\bar{1}10]_{SrNbO_3}$ // $[010]_{SrNbO_{3.4}}$ and $(110)_{SrNbO_3}$ // $(001)_{SrNbO_{3.4}}$, and that their interface is coherent and atomically abrupt. Theoretically, this interface is found to be strongly anisotropic in electronic structure, and takes on quasi-one-dimensional nature. We also find that the interface impacts greatly the electron occupation of Nb *d* orbitals, particularly d_z^2 orbital. The combined study represents a relevant advance in atomically bridging structures to properties of heterointerfaces. © *2014 AIP Publishing LLC*.
[http://dx.doi.org/10.1063/1.4902970]

Strontium niobates of the type $SrNbO_x$ have aroused much interest because their structure and physical properties strongly depend on their oxygen content.[1–15] In general, a very slight modification of the oxygen content in these compounds could result in a remarkable shift in both atomic structure and functionality. The simplest compound in such family is $SrNbO_3$, a perovskite structure comprising of a three-dimensional (3D) network of corner-sharing NbO_6 octahedra with the Sr filling in between the free space.[3] The $SrNbO_3$ in its stoichiometric form has a tetravalent valence state of niobium (Nb^{4+}), is electrically conductive, and has a low 3D isotropic magnetic susceptibility.[4,5] Another interesting compound in this family is $SrNbO_{3.4}$,[6,7] which is derived from 3D network of $SrNbO_3$ perovskite structure by having extra oxygen, separating the NbO_6 octahedra in the direction parallel to {110} plane.[6,7] The excess oxygen atoms modulate the valence state of Nb from the tetravalence (Nb^{4+}) in $SrNbO_3$ to a mixture of tetravalence and pentavalence (Nb^{5+}) in $SrNbO_{3.4}$. In contrast to the perovskite structure, $SrNbO_{3.4}$ has an orthorhombic structure with lattice parameters $a = 3.995$ Å, $b = 5.674$ Å, and $c = 32.356$ Å, in which the NbO_6 octahedra are chainlike connected along the crystallographic *a* axis.[6–8] As a consequence of this unique structure, $SrNbO_{3.4}$ shows an extremely strong anisotropy, rendering it an excellent quasi-1D material.[6–14]

Recently, heterointerfaces between oxides have been extensively studied because they often display unexpected physical properties absent in their bulk constituents.[16] A prototypical example is the discovery of the confined metallic states in between the two band insulators, $SrTiO_3$ and $LaAlO_3$,[17–19] forming a 2D electron gas (2DEG). In addition, ferromagnetic states are also uncovered at an interface between two antiferromagnetic insulators, and a superconducting EG is observed in between two dielectrics.[20–22] To date, a number of mechanisms have been proposed on the emergence of these physical states at oxide heterointerfaces, involving the electronic reconstruction,[18,23] intermixing of cations,[24] and formation of oxygen defects.[25,26] However, to clarify the atomic-scale mechanisms requires experimentally resolving the sites of all the atoms comprising the interface and bridging atomistic structures to their electronic states on a quantum level. In this sense, the determination of interface atomic-scale structures and their associated electronic states not only helps to understand the origins of the discovered phenomena but, in turn, also offers tremendous opportunities for exploring properties in this rapidly emerging field. To this end, we investigate, by combining state-of-the-art transmission electron microscopy (TEM) with atomic first-principles calculations, atomic geometries and electronic states of an interface between the 3D isotropic $SrNbO_3$ and the quasi-1D $SrNbO_{3.4}$, aimed at probing physical properties at the $SrNbO_3/SrNbO_{3.4}$ interface.

The $SrNbO_3/SrNbO_{3.4}$ interface appeared in a crystalline material with composition $SrNbO_{3.32}$, which was grown by the floating zone melting under an Ar atmosphere. The oxygen content of the single crystals was determined by thermogravimetric analysis.[1,6,7] Thin-foil specimens for the TEM and scanning TEM (STEM) imaging were prepared by cutting, grinding, and dimpling the crystal slices down to 20 μm. In a final Ar ion-beam thinning process, we applied an accelerating gun voltage of 2–4 kV and incident beam angle of 4°–7° to avoid radiation damage. Microstructures and orientation relations were taken by the selected-area diffraction pattern (SADP), TEM, and high-resolution TEM (HRTEM) using

[a)]E mail: shlv@wpi-aimr.tohoku.ac.jp
[b)]E mail: zcwang@wpi-aimr.tohoku.ac.jp
[c)]E mail: ikuhara@sigma.t.u-tokyo.ac.jp

JEOL JEM-2010F electron microscope. High-angle annular dark field (HAADF) and annular bright-field (ABF) images were obtained using a 200-kV STEM (JEM-ARM200F, JEOL) equipped with an aberration corrector (CEOS, Gmbh), which offers an unprecedented opportunity to probe structures with sub-Å resolution. Density functional theory (DFT) calculations were carried out using Vienna *ab initio* simulation package (VASP).[27] The projector-augmented wave (PAW) method was employed for the electron-ion interactions,[28] and generalized gradient approximation (GGA) of Perdew *et al.*[29] (PW91) was applied to describe exchange-correlation functional. Single particle Kohn-Sham wave function was expanded using plane wave with a cutoff energy of 500 eV, and irreducible Brillouin zone was sampled with the regular Monkhorst-Pack grid[30] of $8 \times 8 \times 8\,k$ points for bulk $SrNbO_3$, $8 \times 6 \times 2\,k$ points for bulk $SrNbO_{3.4}$, and $6 \times 4 \times 1$ and $8 \times 5 \times 1\,k$ points for the optimization and electronic structure calculations, respectively. All atoms were fully relaxed until the magnitude of force on each atom is less than 0.05 eV/Å.

Figure 1 shows a bright-field (BF) TEM image, a SADP and a HRTEM image of the as-prepared crystal, which is composed of $SrNbO_3$ and $SrNbO_{3.4}$ phases. As shown in Fig. 1(a), the crystal shows a lamellar structure and the major phase is $SrNbO_{3.4}$. The $SrNbO_3$ phase forms very thin lamella with a thickness of a few nanometers (marked by arrows). The interface between $SrNbO_3$ and $SrNbO_{3.4}$ is very flat with no misfit dislocations because they have an extremely low misfit. Figure 1(b) shows a SADP taken at the interfacial region, which is indexed as an overlapping of two sets of diffraction patterns belonging to the $SrNbO_3$ along $[\bar{1}10]$ zone axis (marked by yellow lines) and $SrNbO_{3.4}$ along [010] zone axis (marked by blue lines). These two oxides are determined to have orientation relationships $[\bar{1}10]_{SrNbO_3}$ // $[010]_{SrNbO_{3.4}}$ and $(110)_{SrNbO_3}$ // $(001)_{SrNbO_{3.4}}$. Figure 1(c) shows a typical HRTEM image of the interface, from which one can notice that the interface is atomically abrupt and coherent, and that there appears a periodic image contrast in the $SrNbO_{3.4}$ phase, consistent with its layered structure.

To resolve spatially and identify chemically all atoms at the interface, we conduct an atomic-resolution STEM investigation. Figure 2(a) shows a HAADF STEM image recorded at the interfacial region, in which the interface is confirmed to be coherent and atomically abrupt. Since intensity of an atomic column in the HAADF mode is directly proportional to $Z^{1.7}$ (Z: atomic number),[31] the contrast in the HAADF STEM image is brighter for heavier atoms. This means that the brighter spots represent Nb columns and the relatively darker ones represent Sr columns. However, the much lighter O is not scattered strongly enough to be visualized in the HAADF STEM image, rendering this image incomplete. To directly resolve all atomic columns, we show in Fig. 2(b) an ABF STEM image collected simultaneously with the HAADF STEM image. The ABF STEM technique has been demonstrated to enable a simultaneous imaging of light and heavy atoms with a good signal-to-noise ratio, robustly over a range of specimen thickness.[32] In addition to conveying the identical structural information as in the HAADF image, the ABF STEM image, in which dark spots represent atomic columns, reveals all the atomic columns at the interface including O, which is important for the calculations.

To gain insights into the electronic properties of the $SrNbO_3/SrNbO_{3.4}$ interface, we performed a DFT calculation using the atomic models constructed based on the HAADF and ABF STEM images. To verify the accuracy of our computational methods, we first calculate electronic structures of $SrNbO_3$ (Fig. 3(a)) and $SrNbO_{3.4}$ (Fig. 3(c)) bulks. The calculated densities of states (DOS) for the two bulks using the GGA method are shown in Figs. 3(b) and 3(d). It is noted from Fig. 3(b) that there appear remarkable electronic states at Fermi level (E_F), indicating that electrons can go through E_F. Such a metallicity mainly comes from the Nb d orbitals at E_F which are split into the triply degenerated t_{2g} and the

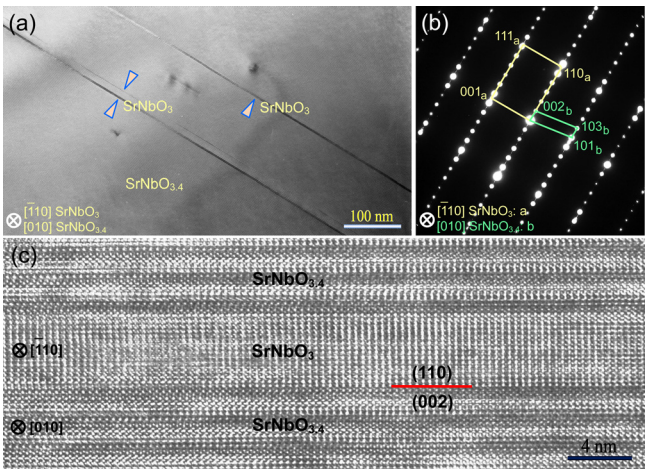

FIG. 1. (a) Bright-field TEM image, (b) SADP, and (c) HRTEM image of the single crystal. The crystal is found to be composed of the $SrNbO_3$ phase and the major phase $SrNbO_{3.4}$. The $SrNbO_3$ phase shows very thin lamella morphology with a thickness of several nanometers, as marked by red arrows. The interface between the $SrNbO_3$ and $SrNbO_{3.4}$ is very flat without any misfit dislocations.

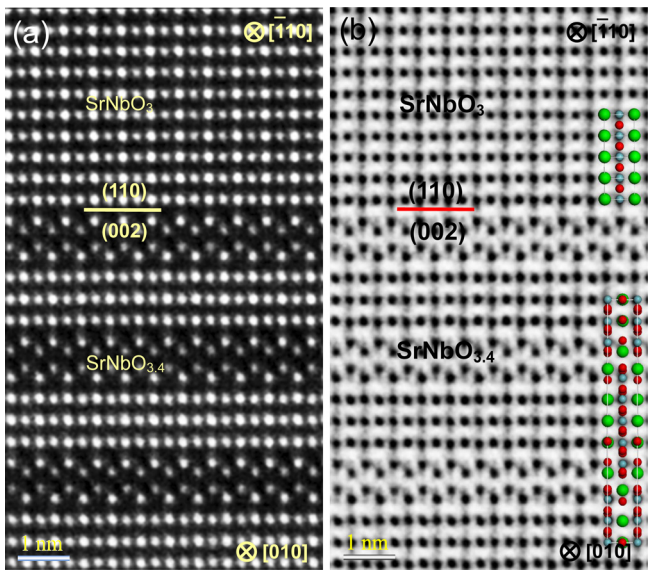

FIG. 2. (a) HAADF and (b) ABF STEM images taken at the interfacial region. The interface is coherent and atomically abrupt. All atomic columns at the $SrNbO_3/SrNbO_{3.4}$ interface including O can be clearly identified in the ABF STEM image. The atomic models of the $SrNbO_3$ and $SrNbO_{3.4}$ are overlaid on to the ABF STEM image.

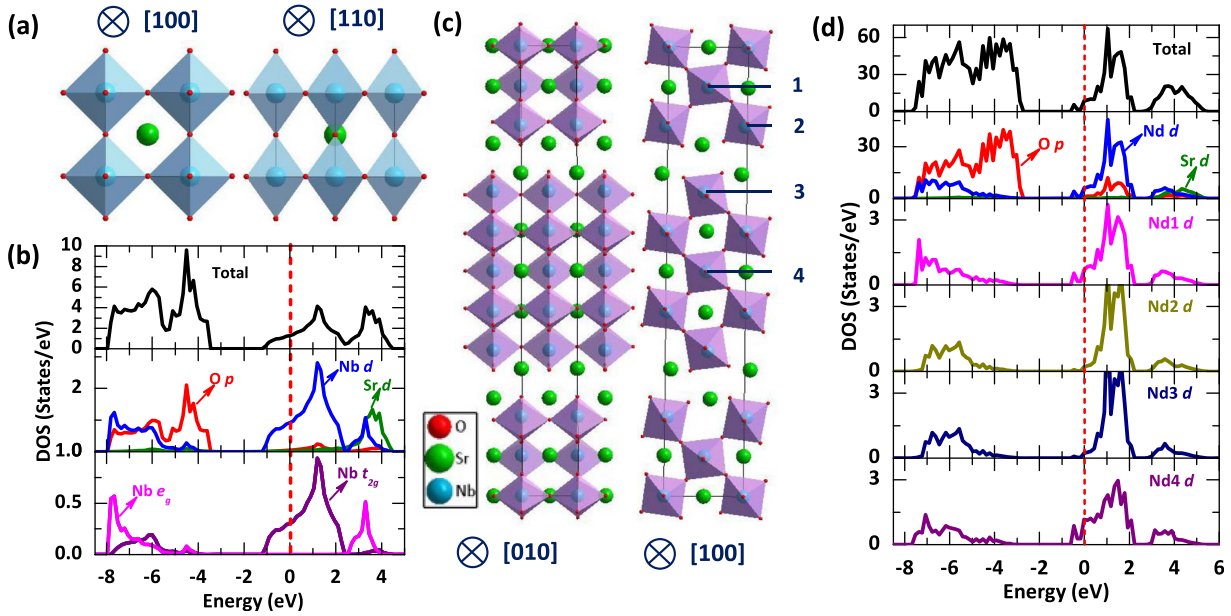

FIG. 3. Optimized structural models for the bulk (a) $SrNbO_3$ and (c) $SrNbO_{3.4}$ viewed from two orthogonal directions. The Nb atoms form an octahedron with its surrounding oxygen atoms. The total and partial DOS are shown for the bulk (b) $SrNbO_3$ and (d) $SrNbO_{3.4}$. The E_F is set to zero and dashed and denoted by vertical lines.

doubly degenerated e_g in the octahedral field, demonstrating little distortion of the NbO_6 octahedra in $SrNbO_3$. The metallicity is also found in $SrNbO_{3.4}$, as electronic states occur at E_F (Fig. 3(d)). Moreover, projected DOS (PDOS) analysis of individual Nb atoms in $SrNbO_{3.4}$ (labeled in Fig. 3(c)) reveals different electronic states at E_F for each of them, which can be attributed to their different valence states arising from the local potential. Hybridization is observed between O p and Nb d states in both $SrNbO_3$ and $SrNbO_{3.4}$, indicating the formation of a covalent bonding between them. To estimate the impact of electron correlations on our calculated results, we also performed calculations using GGA + U, and found results that are similar to those by using the GGA.

Figure 4(a) shows a part of the relaxed interface model, which comprises a $SrNbO_3$ slab of eleven layers and a $SrNbO_{3.4}$ slab of fifteen layers, which are both thick enough to exhibit bulklike properties. Since the tilting of oxygen octahedra plays an important role in electronic reconstruction at the interface, we first analyzed the bond distance and bond angle. For the NbO_6 octahedra on the $SrNbO_{3.4}$ side (Nb3 in Fig. 4(a)), the Nb-O bond lengths are 1.910 Å, 1.864 Å, 2.132 Å, 2.304 Å, 2.061 Å, and 2.057 Å, which do not change

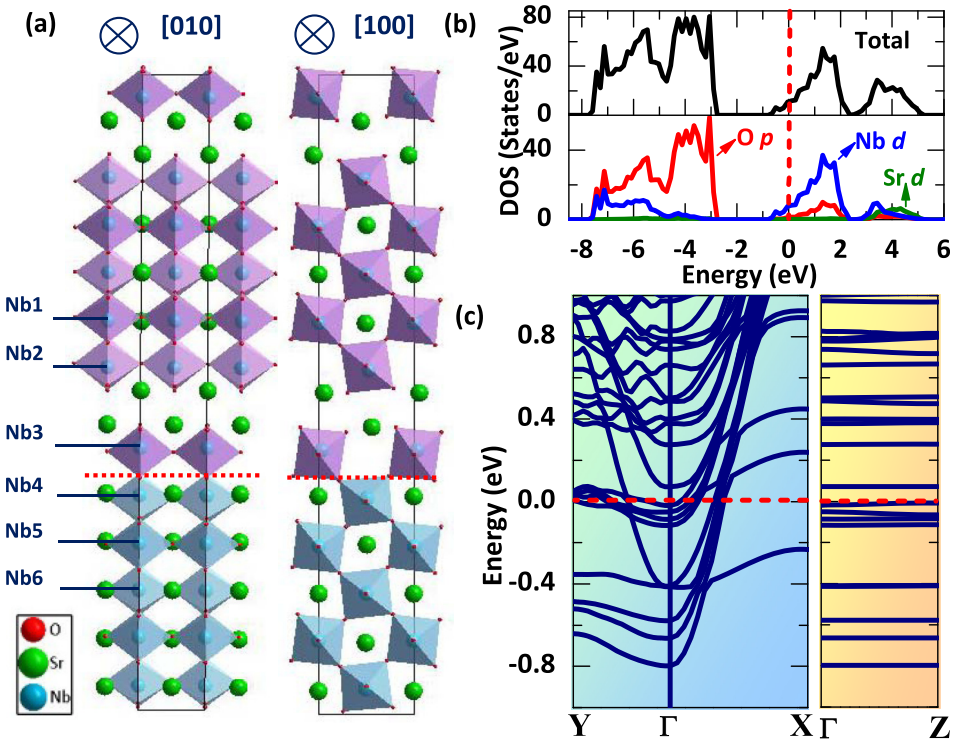

FIG. 4. (a) Energetically stable atomic model for the $SrNbO_3/SrNbO_{3.4}$ interface viewed from two orthogonal directions. The interface is indicated by a horizontal dotted line. The octahedra in the $SrNbO_3$ are highlighted in blue and those in the $SrNbO_{3.4}$ in violet. (b) DOS and (c) band structure of the interface calculated along high-symmetry lines. The E_F is denoted by the dashed lines.

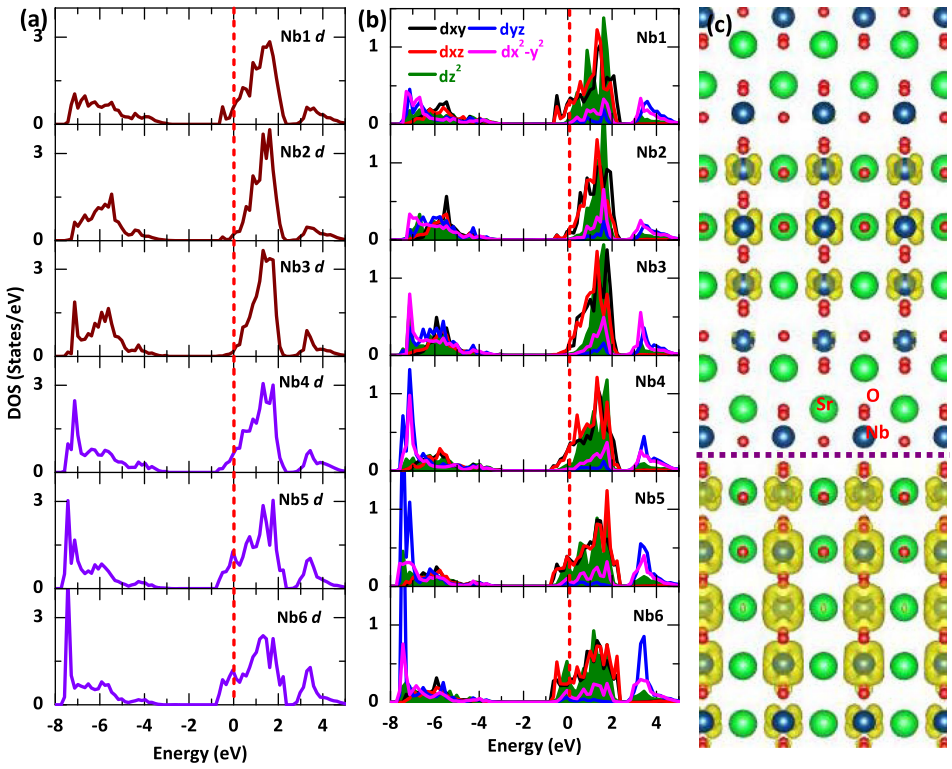

FIG. 5. (a) Partial and (b) orbital-decomposed DOS for several selected Nb atoms near the interface. (c) Charge density isosurface integrated in the energy window ($E_F - 0.7$ eV, E_F) for the $SrNbO_3/SrNbO_{3.4}$ interface viewed along the *b* projection. The interface is marked by a horizontal line, and the atoms that intersect the contour plane are labeled.

markedly from their corresponding bulk values, 1.908 Å, 1.856 Å, 2.118 Å, 2.312 Å, 2.052 Å, and 2.059 Å. However, the bond angles for Nb-O-Nb (Nb3-O-Nb4) across the interface are 152.117° and 177.073°, which change remarkably from the values of 148.140° and 172.164°, respectively, in bulk $SrNbO_{3.4}$, indicating the remarkable tilting of the NbO_6 octahedra (Nb3) at interface. On the other hand, all Nb-O bond distances of the NbO_6 octahedra are the same (2.045 Å) in the $SrNbO_3$ bulk phase, while they are split into different bond distances of 1.995 Å, 1.900 Å, 2.104 Å, 2.175 Å, 2.049 Å, and 2.051 Å on the $SrNbO_3$ side at interface (Nb4 in Fig. 4(a)). Likewise, the Nb-O-Nb angles across the interface are 152.117° and 177.073°, which shift significantly from standard 180° in $SrNbO_3$ bulk. Such a large distortion in the NbO_6 octahedra (Nb4), which is due to the interface effect, makes the five *d* orbitals of Nb4 split completely, thus resulting in different orbital occupation of electrons.

Figure 4(b) presents total and partial DOSs (TDOS and PDOS) of the interface, from which the metallic nature is found to be mainly attributed to Nb *d* states at E_F. To explore electrical properties at different direction, we present in Fig. 4(c) the band structure along the three high-symmetry lines Γ-*X*, Γ-*Y*, and Γ-*Z*. Interestingly, the bands exhibit a quasi-1D dispersion near E_F: there is no discernible dispersion along the Γ-*Y* and Γ-*Z*, yet a strong dispersion along the Γ-*X* (parallel to *a* direction in real space). These indicate that a large electrical anisotropy is present at the $SrNbO_3/SrNbO_{3.4}$ interface, and that the interface behaves like a quasi-1D conductor.

To shed light on the electronic structure of the interfacial Nb atoms, we present in Fig. 5(a) PDOS of several selected Nb atoms (labeled in Fig. 4(a)). In Fig. 5(a), we note that interfacial Nb on the $SrNbO_{3.4}$ side shows a similar DOS as its bulk counterparts: there appear a little yet visible states at E_F for the Nb1, but there are not states at all for the Nb2 and Nb3, indicative of having a valence state of +5. The interfacial Nb on the $SrNbO_3$ side also shows analogous DOS as its bulk counterparts by having a valency of +4. To understand the origin of the anisotropic electrical transport, we conducted an orbital-decomposed PDOS analysis for each Nb atom, as shown in Fig. 5(b). Although the total *d* electron states of the interfacial Nb exhibit a similar character as those in its respective bulk, the orbital-decomposed DOS of each interfacial Nb differs remarkably. The electronic states for the Nb1 at E_F are mainly composed of d_{xy} and d_{xz} orbitals with little contribution from the d_z^2 orbital, and there are almost no electron states at E_F for the Nb2 and Nb3, indicating thereby an anisotropic transport nature.

For the interfacial Nb on the $SrNbO_3$ side, we notice that all the five *d* orbitals of Nb6 contribute to the electronic states at E_F, which demonstrates an isotropic electrical transport. The contribution of the d_z^2 orbital to electron states at E_F is gradually lessened from the sub-interfacial Nb5 to the interfacial Nb4, which is attributed to the interfacial effect, demonstrating that interface can have an influence on orbital occupations of Nb and hence the electrical transport. Figure 5(c) shows an electron-density isosurface for the electronic states near E_F, revealing unambiguously confinement of charges on the $SrNbO_{3.4}$ side: the charges are dominantly localized at the central Nb layer of $SrNbO_{3.4}$ supercell with a small degree of leakage to its two neighboring Nb layers. Moreover, the number of charges on the $SrNbO_3$ side decreases gradually when approaching interface, consistent with the PDOS analysis.

Summing up, we have conducted a combined investigation of transmission electron microscopy and first-principles calculations to the $SrNbO_3/SrNbO_{3.4}$ interface, aimed at probing its atomic-scale structure and electronic properties.

The orientation relationship between the $SrNbO_3$ and $SrNbO_{3.4}$ is determined as $[\bar{1}10]_{SrNbO_3}$ // $[010]_{SrNbO_{3.4}}$ and $(110)_{SrNbO_3}$ // $(001)_{SrNbO_{3.4}}$. Further atomic-resolution imaging reveals that the heterointerface is epitaxial, coherent, and atomically abrupt with no clear evidence of misfit dislocations. The band structure calculations reveal a strongly anisotropic electrical transport and a quasi-1D nature for the $SrNbO_3/SrNbO_{3.4}$ interface. We also find that the interface can have a marked influence on the electron occupation of Nb *d* orbitals, particularly the d_z^2 orbital. Such a combined study sheds light on atomistic structure and unique electronic properties of heterointerfaces, which is relevant for the fundamental scientific research on interfaces.

This work was conducted in part at the Research Hub for the Advanced Nano Characterization and "Nanotechnology Platform" at the University of Tokyo supported by MEXT of Japan, and was supported in part by the Elements Strategy Initiative for Structural Materials (ESISM) *via* MEXT by Japan and JSPS Grant-in-Aid for Scientific Research on Innovative Areas "Nano Informatics." C.C. acknowledges support from the Grant-in-Aid for Young Scientists (B) (Grant No. 26820288). Z.W. thanks the financial support from the Grant-in-Aid for Young Scientists (A) (Grant No. 24686069), the NSFC (Grant No. 11332013), the JSPS and CAS under the Japan-China Scientific Cooperation Program, and the Murata Science Foundation. F.L. thanks Nicola Spaldin for her support. Calculations were conducted at the ISSP, University of Tokyo.

[1]F. Lichtenberg, T. Williams, A. Reller, D. Widmer, and J. G. Bednorz, Z. Phys. B: Condens. Matter **84**, 369 (1991).
[2]D. Liu, X. Yao, and D. M. Smyth, Mater. Res. Bull. **27**, 387 (1992).
[3]D. Ridgley and R. Ward, J. Am. Chem. Soc. **77**, 6132 (1955).
[4]S. A. Turzhevsky, D. L. Novikov, V. A. Gubanov, and A. J. Freeman, Phys. Rev. B **50**, 3200 (1994).
[5]K. Isawa, R. Itti, J. Sugiyama, N. Koshizuka, and H. Yamauchi, Phys. Rev. B **49**, 3534 (1994).
[6]F. Lichtenberg, A. Herrnberger, K. Wiedenmann, and J. Mannhart, Prog. Solid State Chem. **29**, 1 (2001).
[7]F. Lichtenberg, A. Herrnberger, and K. Wiedenmann, Prog. Solid State Chem. **36**, 253 (2008).
[8]S. C. Abrahams, H. W. Schmalle, T. Williams, A. Reller, F. Lichtenberg, D. Widmer, J. G. Bednorz, R. Spreiter, Ch. Bosshard, and P. Günter, Acta Crystallogr. B **54**, 399 (1998).
[9]A. de Campos, M. S. Da Luz, C. A. M. Dos Santos, A. T. Rice, A. M. Deml, B. D. White, J. J. Neumeier, and J. L. Cohn, Phys. Rev. B **82**, 125117 (2010).
[10]C. A. Kuntscher, S. Schuppler, P. Haas, B. Gorshunov, M. Dressel, M. Grioni, F. Lichtenberg, A. Herrnberger, F. Mayr, and J. Mannhart, Phys. Rev. Lett. **89**, 236403 (2002).
[11]A. Sakai, T. Kanno, K. Takahashi, Y. Yamada, and H. Adachi, J. Appl. Phys. **108**, 103706 (2010).
[12]J. E. Weber, C. Kegler, N. Buttgen, H. A. Krug von Nidda, A. Loidl, and F. Lichtenberg, Phys. Rev. B **64**, 235414 (2001).
[13]W. Kobayashi, Y. Hayashi, M. Matsushita, Y. Yamamoto, I. Terasaki, A. Nakao, H. Nakao, Y. Murakami, Y. Moritomo, H. Yamauchi, and M. Karppinen, Phys. Rev. B **84**, 085118 (2011).
[14]C. A. Kuntscher, S. Schuppler, P. Haas, B. Gorshunov, M. Dressel, M. Grioni, and F. Lichtenberg, Phys. Rev. B **70**, 245123 (2004).
[15]C. A. Kuntscher, S. Gerhold, N. Nucker, T. R. Cummins, D. H. Lu, S. Schuppler, C. S. Gopinath, F. Lichtenberg, J. Mannhart, and K. P. Bohnen, Phys. Rev. B **61**, 1876 (2000).
[16]H. Y. Hwang, Y. Iwasa, M. Kawasaki, B. Keimer, N. Nagaosa, and Y. Tokura, Nat. Mater. **11**, 103 (2012).
[17]S. Okamoto and A. J. Millis, Nature **428**, 630 (2004).
[18]A. Ohtomo and H. Y. Hwang, Nature **427**, 423 (2004).
[19]S. Thiel, G. Hammerl, A. Schmeh, C. W. Schneider, and J. Mannhart, Science **313**, 1942 (2006).
[20]P. A. Salvador, A. M. Haghiri-Gosnet, B. Mercey, M. Hervieu, and B. Raveau, Appl. Phys. Lett. **75**, 2638 (1999).
[21]A. Gozar, G. Logvenov, L. F. Kourkoutis, A. T. Bollinger, L. A. Giannuzzi, D. A. Muller, and I. Bozovic, Nature **455**, 782 (2008).
[22]N. Reyren, S. Thiel, A. D. Caviglia, L. F. Kourkoutis, G. Hammerl, C. Richter, C. W. Schneider, T. Kopp, A. S. Rüetschi, D. Jaccard, M. Gabay, D. A. Muller, J. M. Triscone, and J. Mannhart, Science **317**, 1196 (2007).
[23]N. Nakagawa, H. Y. Hwang, and D. A. Muller, Nat. Mater. **5**, 204 (2006).
[24]P. R. Willmott, S. A. Pauli, R. Herger, C. M. Schleputz, D. Martoccia, B. D. Patterson, B. Relley, R. Clarke, D. Kumah, C. Cionca, and Y. Yacoby, Phys. Rev. Lett. **99**, 155502 (2007).
[25]G. Herranz, M. Basletic, M. Bibes, C. Carrétéro, E. Tafra, E. Jacquet, K. Bouzehouane, C. Deranlot, A. Hamzic, J. M. Broto, A. Barthélémy, and A. Fert, Phys. Rev. Lett. **98**, 216803 (2007).
[26]W. Siemons, G. Koster, H. Yamamoto, W. A. Harrison, G. Lucovsky, T. H. Geballe, D. H. A. Blank, and M. R. Beasley, Phys. Rev. Lett. **98**, 196802 (2007).
[27]G. Kresse and J. Hafner, Phys. Rev. B **47**, 558 (1993).
[28]P. E. Blöchl, Phys. Rev. B **50**, 17953 (1994).
[29]J. P. Perdew, J. A. Chevary, S. H. Vosko, K. A. Jackson, M. R. Pederson, D. J. Singh, and C. Fiolhais, Phys. Rev. B **46**, 6671 (1992).
[30]H. J. Monkhorst and J. D. Pack, Phys. Rev. B **13**, 5188 (1976).
[31]S. J. Pennycook and L. A. Boatner, Nature **336**, 565 (1988).
[32]S. D. Findlay, N. Shibata, H. Sawada, E. Okunishi, Y. Kondo, T. Yamamoto, and Y. Ikuhara, Appl. Phys. Lett. **95**, 191913 (2009).